INVESTIGATION OF CONVENTIONAL DNAFETS FOR GENOME-WIDE DETECTION OF POLYMORPHISMS

Clemens Heitzinger* **and Gerhard Klimeck**

Network for Computational Nanotechnology
School of Electrical and Computer Engineering
Purdue University, West Lafayette, IN 47907, USA

*Corresponding author: Clemens Heitzinger
Phone: +1(765)494-5589, fax: +1(765)494-6441, e-mail: ClemensH@Purdue.edu

Abstract: Conventional SOI DNAFET devices, being able to detect single-nucleotide polymorphisms, are simulated in a comprehensive approach. These devices can be fabricated in high-density arrays and offer advantages compared to optical detection methods. The influence of device parameters like doping concentration and the size of the exposed sensor area is investigated.
Keywords: BioFET, DNAFET, simulation.

INTRODUCTION

A BioFET (biologically sensitive field-effect transistor) is a MOSFET whose conventional gate structure is replaced by immobilized probe molecules [1]. This idea can be traced back to the ISFET device structure [2, 3]. A DNAFET is a special case of a BioFET where ssDNA (single-stranded DNA) oligomers act as probe molecules (see Fig. 1). As target molecules (i.e., complementary ssDNA) bind to the probe molecules, the additional charge of the complementary strands modulates the charge transport in the semiconductor transducer and the resulting conductance change enables detection. These biosensors are very promising for DNA sequencing, for detecting single-nucleotide polymorphisms, for detecting small interfering RNA, and for detecting cancer markers. Eventually point-of-care devices can be built on semiconductor sensors.

The main advantages of DNAFET arrays compared to optical detection methods like DNA microarrays based on fluorescence is that detection works label-free and that signal-processing can be performed in-silico. Hence the process step of marking the target molecule becomes unnecessary, as well as the final image processing step, which is the main bottle-neck of optical methods.

DNAFETs with silicon-nanowire transducers were reported in [4]. Although the vapor-liquid-solid growth mechanism of silicon whiskers has been known since the 1960s and whiskers with 100nm diameter were already grown at that time [5], epitaxial growth of silicon-nanowires has never been demonstrated. Recently we investigated the technological limits of silicon-nanowire DNAFETs due to the Debye length of the charges of the target molecules [6, 7]. The fundamental problem of BioFETs, especially when operating at physiological conditions, is that the Debye length decreases rapidly with increasing salt concentration; still, a certain amount of Na^+Cl^- is necessary for DNA hybridization (see Fig. 2).

Here we investigate conventional DNAFET structures, derived from the SOI MOSFET structure, since they can be manufactured reliably in large arrays and hence are the building blocks for detecting single-nucleotide polymorphisms in large genomes.

Considering the example of S. cerevisiae, its whole genome consists of 12 156 590 nucleotides. If we assume 25-nucleotide oligomer probes at a spacing of 5 base-pairs [8], about $2.5 \cdot 10^6$ sensor sites are necessary to cover the whole genome. Each sensor site consists of a MOSFET and a signal-processing circuit. Adding space for interconnects and read-out lines, an estimated area of $10\mu\mathrm{m} \cdot 10\mu\mathrm{m}$ is necessary for each sensor, and therefore it is estimated that a genome-wide polymorphism detector can be fitted within a square with a side length of $\sqrt{2.5 \cdot 10^6} \cdot 10\mu\mathrm{m} \approx 16\mathrm{mm}$.

In the following the simulation method is described and the approach is used to investigate and optimize device parameters.

SIMULATION METHOD

The simulation approach employed here is both rigorous and comprehensive. It starts at the feature-scale level and does not contain any fitting parameters. After constructing the ssDNA and dsDNA oligomers from the coordinates of the single base-pairs [9], the partial charges are determined using a GROMACS force-field [10, 11]. After completing the feature-scale structure by

adding the insulator and semiconductor domains, and rotating it if necessary, the Poisson–Boltzmann equation is solved to obtain the electrostatic potential [12] (see Figures 3 and 4). Furthermore the potential shift due to the surface charge double-layer is $\approx -0.165\mathrm{V}$ for silicon oxide in water at a pH value of 7.

In the case of silicon-nanowire devices, charge transport is calculated using the non-equilibrium Green function formalism [13] in a self-consistent simulator. Silicon-nanowire DNAFETs are more sensitive due to their larger surface-to-volume ratio.

In the case of conventional SOI devices, i.e., conducting nanoplates of silicon, the potential shift at the insulator surface is determined, and a compact model for a $0.25\mu\mathrm{m}$-MOSFET is used to obtain the output characteristics [14]. In addition the well-known MiniMOS 6.1 device simulator is used for more accurate results [15]. Using MiniMOS the output characteristics are calculated and a small-signal AC analysis is performed to determine the conductance of the nanoplate. In experiments usually the conductance values are measured using a lock-in amplifier.

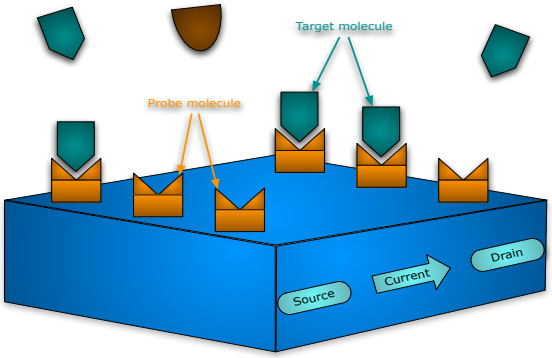

Figure 1: This figure shows the schematic diagram of BioFETs. The semiconductor transducer is covered with a thin oxide (or nitride) layer. Probe molecules are immobilized to the surface. The conductance of the transducer is measured, e.g., using a lock-in amplifier.

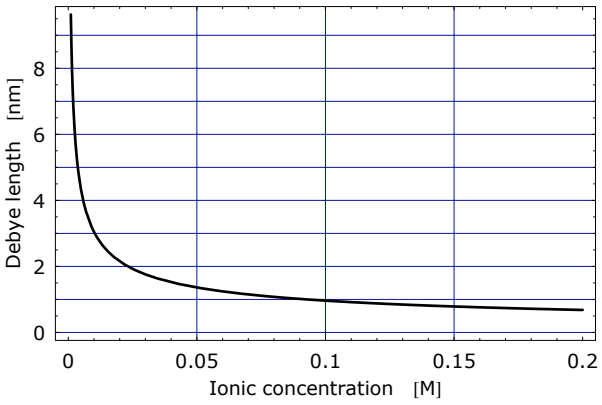

Figure 2: The Debye length as a function of $\mathrm{Na}^{+}\mathrm{Cl}^{-}$ concentration. Physiological conditions correspond to a concentration of $\approx 150\mathrm{mM}$.

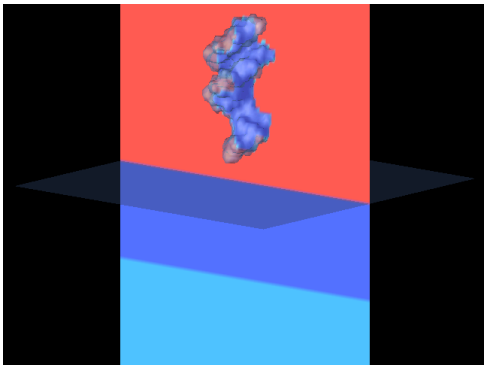

Figure 3: This figure illustrates the feature-scale simulations. The red domain is the aqueous solution, the blue domain is the silicon dioxide layer, and the cyan domain is the bulk silicon. The transparent grey plane is the boundary whose electrostatic boundary conditions are used in the transport simulation. A 12-base-pair dsDNA oligomer is also shown.

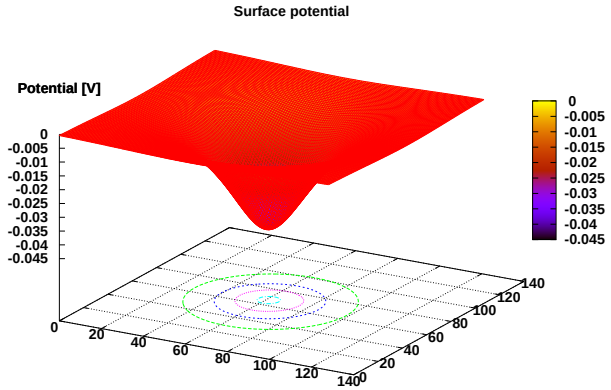

Figure 4: This figure shows the surface potential for a 12-base-pair single-stranded oligomer at a probe spacing of 7nm and normal to the surface. The average potential change is $-0.00454\mathrm{V}$ for the single strand and $-0.00769\mathrm{V}$ for the double strand.

RESULTS AND DISCUSSION

In general there are three states of a BioFET that are of interest. Firstly no probe molecules are attached to the transducer, secondly a functioning sensor is produced by immobilizing probe molecules on the transducer surface, and thirdly target molecules are attached to a certain percentage of the probe sites. The main goal is to maximize the sensitivity of the device.

In the first example the influence of the active sensor area is investigated. The areas exposed to the solution are squares with side lengths varying from $500\mathrm{nm}$ to $4000\mathrm{nm}$. The probe strands have the sequence CGT-GAA-TTC-ACG and are located parallel to the surface at a distance of 1nm. The oxide layer is $4\mathrm{nm}$ thick, and the spacing between the probe strands is $7\mathrm{nm}$ in each direction which results in a binding efficiency of

nearly 100%. The solution is $10\mathrm{mM}$ Na^+Cl^- at a pH value of 7. The small-signal AC analysis is performed for $50\mathrm{mV}$ at $79\mathrm{Hz}$.

Fig. 5 and Fig. 6 show the resulting conductances for different binding efficiencies. The absolute conductance values increase rapidly for devices with a side length smaller than $2000\mathrm{nm}$. The relative conductance change, which is more important in experiments than the absolute change, is noticeably reduced for the device with a side length of $500\mathrm{nm}$. This implies that as devices are scaled down, the binding efficiencies become are crucial factor for the sensitivity of the device.

In the second example the influence of the phosphorus source and drain implantation dose of on device behavior is studied. The device here is the same as in the first example with a sensor area side length of $4000\mathrm{nm}$. Fig. 7 and Fig. 8 show the absolute and relative conductance changes. The absolute conductance values increase with doping concentration. The relative change is not as profound, but significant, and means that higher doping yields higher sensitivity. The source and drain implantation dose is also important regarding the resistance at the metal contacts.

The third example is concerned with the influence of the dose of the channel implantation. We study the same device as in the first example where it has no channel implant, but vary the dose of the boron channel implantation in this example. Fig. 9 and Fig. 10 show the results. For higher implantation doses the absolute values decrease, whereas the relative values increase. Hence higher doping concentrations result in higher sensitivity.

CONCLUSIONS

We presented a rigorous simulation approach that contains no fitting parameters. It shows very good agreement with experimental results and hence the simulations imply that the functioning of DNAFETs can indeed be understood in terms of the field-effect due to the partial charges of the target molecules, and that experimental data are not due to other, parasitic, effects. The simulation results show that in this kind of device engineering trade-offs regarding the measurement setup exist. Guidance for future experiments is provided by the simulations. To facilitate the interaction between theorists and experimentalists, the simulator for conventional and silicon-nanowire DNAFETs is available online at http://www.nanohub.org (see Fig. 11).

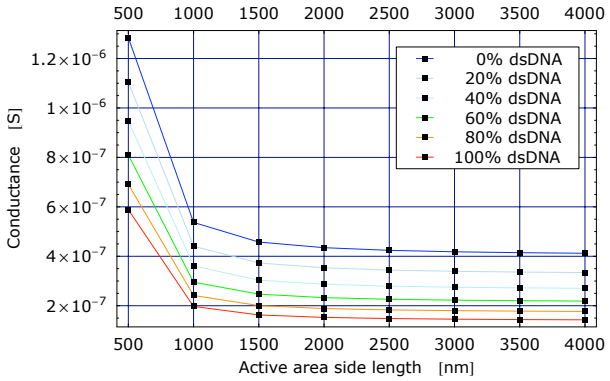

Figure 5: The absolute conductance values as a function of active area side length and of binding efficiency.

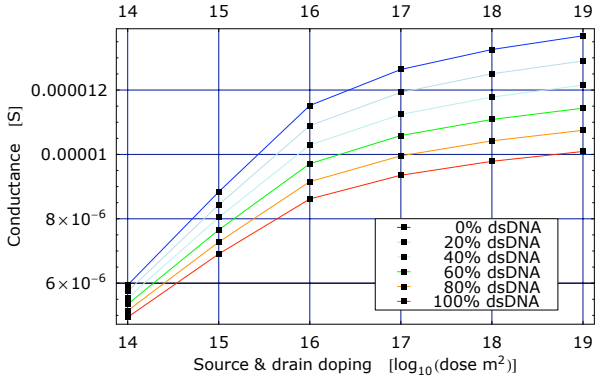

Figure 7: The absolute conductance values as a function of phosphorus source and drain implantation dose and of binding efficiency.

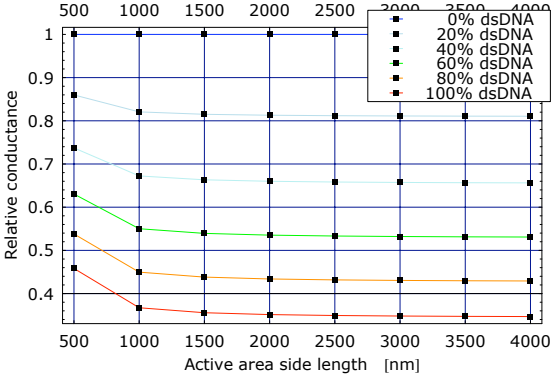

Figure 6: The relative conductance change as in Fig. 5 with respect to a baseline of 0% dsDNA.

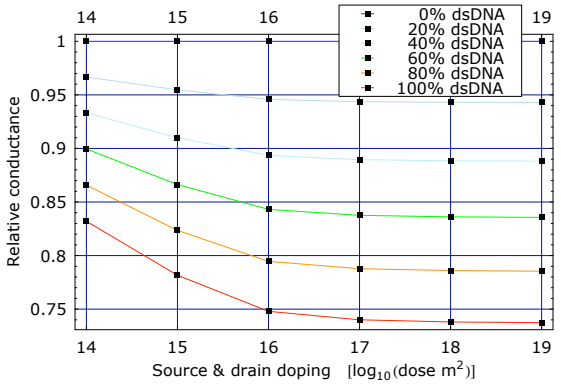

Figure 8: The relative conductance change as in Fig. 7 with respect to a baseline of 0% dsDNA.

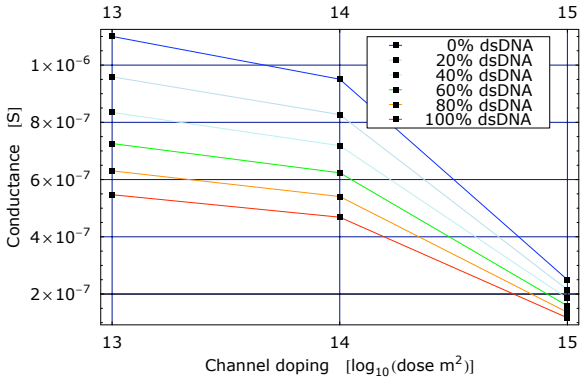

Figure 9: The absolute conductance values as a function of boron channel implantation dose and of binding efficiency.

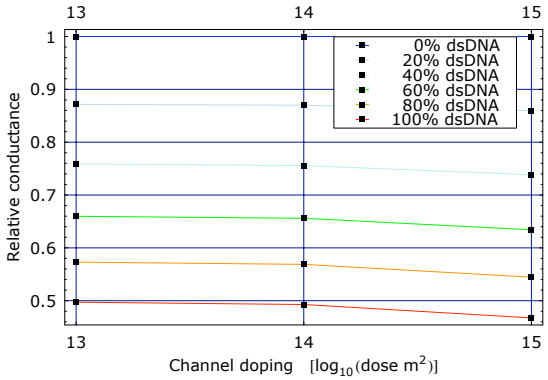

Figure 10: The relative conductance change as in Fig. 9 with respect to a baseline of 0% dsDNA.

ACKNOWLEDGMENT

This material is based upon work supported by the National Science Foundation under Grant No. EEC-0228390, the Indiana 21st Century fund, and the Semiconductor Research Corporation. The authors thank Siegfried Selberherr for providing the MiniMOS 6.1 source code, and Ashraf Alam, Rashid Bashir, and Oguz Elibol for discussions on experimental setups.

REFERENCES

[1] M.J. Schöning and A. Poghossian. Recent advances in biologically sensitive field-effect transistors (BioFETs). *Analyst*, 127:1137–1151, 2002.

[2] P. Bergveld. Development of an ion-sensitive solid-state device for neurophysiological measurements. *IEEE Trans. Biomed. Eng.*, BME-17:70–71, 1970.

[3] P. Bergveld. Development, operation and application of the ion sensitive field effect transistor as a tool for electrophysiology. *IEEE Trans. Biomed. Eng.*, BME-19:342–351, 1972.

[4] J. Hahm and C.M. Lieber. Direct ultrasensitive electrical detection of DNA and DNA sequence variations using nanowire nanosensors. *Nano Lett.*, 4(1):51–54, 2004.

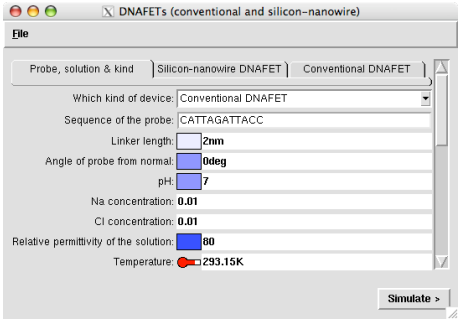

Figure 11: In online simulations the user can change parameters of the solution, the device sizes and dopings, the applied voltages, and so forth.

[5] R.S. Wagner and W.C. Ellis. Vapor-liquid-solid mechanism of single crystal growth. *Appl. Phys. Lett.*, 4(5):89–90, 1964.

[6] Clemens Heitzinger and Gerhard Klimeck. Simulation study of silicon-nanowire field-effect DNA-sensors. In *Proc. International Congress on Nanobiotechnology and Nanomedicine (NanoBio 2006)*, San Francisco, CA, USA, June 2006.

[7] Clemens Heitzinger and Gerhard Klimeck. Numerical aspects of the three-dimensional feature-scale simulation of silicon-nanowire field-effect sensors for DNA detection. In *Proc. 11th International Workshop on Computational Electronics (IWCE 11)*, Vienna, Austria, May 2006. IEEE.

[8] D. Gresham, D.M. Ruderfer, S.C. Pratt, J. Schacherer, M.J. Dunham, D. Botstein, and L. Kruglyak. Genome-wide detection of polymorphisms at nucleotide resolution with a single DNA microarray. *Science*, 311:1932–1936, March 2006.

[9] S. Premilat and G. Albiser. Conformations of A-DNA and B-DNA in agreement with fiber X-ray and infrared dichroism. *Nucleic Acids Res.*, 11(6):1897–1908, March 1983.

[10] D. Eisenberg and A.D. McLachlan. Solvation energy in protein folding and binding. *Nature*, 319:199–203, January 1986.

[11] D. van der Spoel, E. Lindahl, B. Hess, A.R. van Buuren, E. Apol, P.J. Meulenhoff, D.P. Tieleman, A.L.T.M. Sijbers, K.A. Feenstra, R. van Drunen, and H.J.C. Berendsen. *Gromacs User Manual version 3.2*, 2004. http://www.gromacs.org.

[12] N.A. Baker, D. Sept, S. Joseph, M.J. Holst, and J.A. McCammon. Electrostatics of nanosystems: Application to microtubules and the ribosome. *Proc. Nat. Acad. Sci. U.S.A.*, 98(18):10037–10041, August 2001.

[13] S. Datta. *Quantum Transport: Atom to Transistor*. Cambridge University Press, Cambridge, 2nd edition, 2005.

[14] T. Sakurai and A. Newton. A simple MOSFET model for circuit analysis. *IEEE Trans. El. Dev.*, 38(4):887–894, April 1991.

[15] S. Selberherr et al. *MiniMOS 6.1 Users's Guide*. Institute for Microelectronics, Technical University Vienna, Vienna, Austria, July 1999.